A Review of the Total Field/Scattered Field Technique for the FDTD Method

Mike Potter * and Jean-Pierre Bérenger **

* Electrical and Computer Engineering
University of Calgary, Canada
(Email: mpotter@ucalgary.ca)

** School of Electrical and Electronic Engineering
The University of Manchester, UK
(Email: jpberenger@gmail.com)

***Abstract*—The Total Field/ Scattered Field method, also called the Huygens surface method, was introduced more than three decades ago to impress an incident plane wave in the computational domain of the finite-difference time-domain (FDTD) method. It is now a basic feature of FDTD softwares. This paper summarizes the principle of the method and reviews the improvements and extensions added over the years to reduce the spurious effect of the FDTD dispersion and to apply the method in various contexts.**

***Index Terms*—FDTD, total field, scattered field, TF/SF, Huygens surface, plane wave, auxiliary equation.**

I. Introduction

Many problems solved with the finite-difference time-domain (FDTD) method consist of computing the interaction of an incident wave with objects or structures located within the computational domain. Solving such problems implies that the incident wave, in most cases a plane wave, must be generated within the FDTD domain. This was a challenging question in the early times of the use of the FDTD method, because a FDTD domain is finite in size while a plane wave is infinite in the directions perpendicular to the propagation. Before 1980, the difficulty was overcome by computing the scattered field in place of the total field [1, 2, 3], which permits the incident wave to be replaced by current sources on the surface or within the scattering objects. However, with this method the dynamic range in the FDTD domain was severely limited by the FDTD noise. A better method, the Total Field/Scattered Field (TF/SF) method, also called the Huygens surface method, was reported for the first time in [4], and later in [5] and [6]. It consists of replacing the incident wave with sources placed on a fictitious surface surrounding the region of interest. The total field is then present within the closed surface while only the scattered field is present outside it. This is well suited to open problems where the field that strikes the absorbing boundary conditions is then only the outgoing scattered field.

The total field/scattered field method is nowadays of general use in the numerous applications of the FDTD method where an incident field is produced by sources located outside the computational domain. It is now a basic feature of FDTD simulation softwares. Over the years, some improvements and extensions of the method have been introduced. Firstly the spurious effects of the dispersion of the FDTD method on the field generated by the Huygens surface has been reduced by developing auxiliary equations methods that permit the enforced incident wave to better match the dispersion of the FDTD grid. This dramatically reduces the noise produced by the Huygens surface. Secondly the method has been implemented in other media than in a vacuum, and it has been used in other contexts than the usual generation of an incident plane wave.

The first part of the paper summarizes the principle and the implementation of the method in the case of a FDTD domain filled with a vacuum. The second part reviews the methods developed in the past two decades to reduce the spurious effect of the dispersion, which permits extremely high dynamic range to be achieved in the computational domain. The third part reviews some extensions of the method to other media and its use in various contexts, comprising of (i) extensions of the method to such media as absorbing media, dispersive media, and layered media; and (ii) its use in various contexts to replace sources located in the FDTD domain, to connect several FDTD grids, and to generate evanescent waves.

II. The Total Field/Scattered Field Method

Let us denote as the incident field (E_{inc}, H_{inc}) the field produced inside a space domain by sources placed outside it. If a scattering object or any other modification of the medium is introduced in the domain, the field differs from the incident field, it is called the total field (E_{tot} ,H_{tot}). The scattered field (E_{scat}, H_{scat}) is, by definition, the difference of the two fields

$$\vec{E}_{scat} = \vec{E}_{tot} - \vec{E}_{inc} \quad (1\text{-a})$$

$$\vec{H}_{scat} = \vec{H}_{tot} - \vec{H}_{inc} \quad (1\text{-b})$$

With the total field/scattered field method [4, 5, 6] there are two regions in the FDTD domain, an interior region where the field is (E_{tot}, H_{tot}), and an exterior region where the field is (E_{scat}, H_{scat}). The incident wave is impressed by a modification of the FDTD equations near the surface separating the two regions, which physically corresponds to the replacement of the incident wave with fictitious current sheets depending on (E_{inc}, H_{inc}) on that surface.

II-1. The Total field/Scattered field method in the FDTD grid.

Let us consider the two dimensional (2D) FDTD domain in Fig.1, in the case of the TE mode where the field components are E_x, E_y, and H_z. The domain is separated into two parts by an artificial line situated between columns *is*-1/2 and *is*. Let us assume that the E field at time step n and the H field at time step n+1/2 are the scattered field in the left-hand part and the total field in the right-hand part. The objective is the advance of the FDTD marching-in-time problem by one time step while preserving the scattered and total fields in their respective regions.

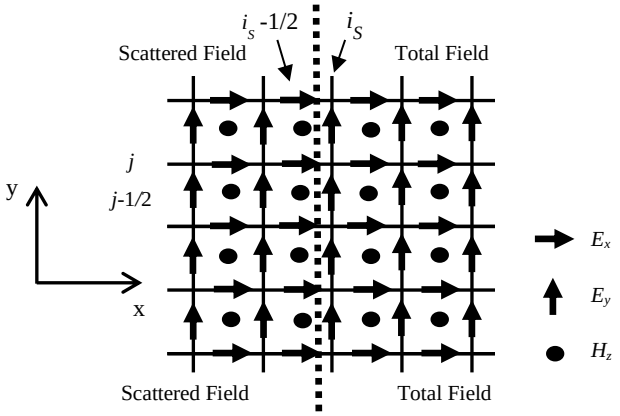

Fig. 1. Scattered and Total field regions separated with a vertical line in a 2D FDTD domain.

The FDTD equation of the advance of E_y in the 2D grid reads

$$E_y^{n+1}(i, j+1/2) = E_y^n(i, j+1/2) - \frac{\Delta t}{\varepsilon_0 \Delta x}\left[H_z^{n+1/2}(i+1/2, j+1/2) - H_z^{n+1/2}(i-1/2, j+1/2)\right] \quad (2)$$

At E_y nodes where $i < is$, the two H_z nodes in the derivative on space in (2) are in the scattered field region. From this, using (2) the advanced E_y is a scattered field. Similarly, at nodes $i > is$ the two H_z nodes in (2) are in the total field region, so that the advanced E_y is a total field. Equation (2) thus produces the desired field, either a scattered field or a total field, at any E_y node where $i \neq is$. Conversely, at nodes where $i = is$ which are in the total field region, (2) cannot be used as it stands. Because $H_z(is\text{-}1/2, j\text{+}1/2)$ is in the scattered field region while $H_z(is\text{+}1/2, j\text{+}1/2)$ is in the total field region. The discrete derivative in (2) is meaningless. However, a total field derivative can be obtained by adding the known incident field $H_{z\_inc}(is\text{-}1/2, j\text{+}1/2)$ to the scattered field $H_z(is\text{-}1/2, j\text{+}1/2)$ present in the grid. That is by replacing (2) with the following equation which then produces the desired total field E_y at time n+1:

$$E_y^{n+1}(is, j+1/2) = E_y^n(is, j+1/2) - \frac{\Delta t}{\varepsilon_0 \Delta x}\left[H_z^{n+1/2}(is+1/2, j+1/2) - \left\{H_z^{n+1/2}(is-1/2, j+1/2) + H_{z\_inc}^{n+1/2}(is-1/2, j+1/2)\right\}\right] \quad (3)$$

For the advance of the H_z component, the situation is similar. The regular FDTD equation

$$H_z^{n+1/2}(i-1/2, j+1/2) = H_z^{n+1/2}(i-1/2, j+1/2) - \frac{\Delta t}{\mu_0 \Delta x}\left[E_y^n(i, j+1/2) - E_y^n(i-1, j+1/2)\right] + \frac{\Delta t}{\mu_0 \Delta y}\left[E_x^n(i-1/2, j+1) - E_x^n(i-1/2, j)\right] \quad (4)$$

can be used to advance the scattered H_z at nodes where $i < is$-1/2 and the total H_z at nodes where $i > is$-1/2. But at nodes $H_z(is\text{-}1/2, j\text{+}1/2)$, the x-directed derivative in (4) involves $E_y(is\text{-}1, j\text{+}1/2)$ in the scattered field region and $E_y(is, j\text{+}1/2)$ in the total field region. Equation (4) cannot be used. The incident field $E_{y\_inc}(is, j\text{+}1/2)$ must be subtracted to the total field $E_y(is, j\text{+}1/2)$ to obtain a scattered derivative. This yields the equation that permits the desired scattered field H_z to be advanced on time

$$H_z^{n+1/2}(is-1/2, j+1/2) = H_z^{n-1/2}(is-1/2, j+1/2) - \frac{\Delta t}{\mu_0 \Delta x}\left[\left\{E_y^n(is, j+1/2) - E_{y\_inc}^n(is, j+1/2)\right\} - E_y^n(is-1, j+1/2)\right] + \frac{\Delta t}{\mu_0 \Delta y}\left[E_x^n(i-1/2, j+1) - E_x^n(i-1/2, j)\right] \quad (5)$$

Concerning the E_x component, its FDTD equation only involves a derivative of H_z in y direction, i.e. in the direction parallel to the separation of the scattered and total field regions. In particular, at nodes $E_x(is\text{-}1/2, j)$ the derivative on space involves $H_z(is\text{-}1/2, j\text{+}1/2)$ and $H_z(is\text{-}1/2, j\text{-}1/2)$. Both are in the scattered field region, so that the regular FDTD equation produces the desired scattered field $E_x(is\text{-}1/2, j)$. This regular equation can be used at any other node of the grid without modification.

The modification of the FDTD equations described for a separation in the x direction in Fig. 1 can be transposed in a trivial manner to a separation in y direction. Fig. 2 shows the upper-left part of a rectangular separation of a FDTD domain with a total field region in the interior of the rectangle and a scattered field region outside it. The vertical separation in Fig. 2a) is like the one in Fig. 1, i.e. equations (3) and (5) can be applied. For the advances of $E_x(i\text{+}1/2, js)$ and $H_z(i\text{+}1/2, js\text{+}1/2)$ which involve discrete derivatives in y direction, equations similar to (3) and (5) can be obtained. Here $H_{z\_inc}(i\text{+}1/2, js\text{+}1/2)$ is added to $H_z(i\text{+}1/2, js\text{+}1/2)$ for the advance of $E_x(i\text{+}1/2, js)$, and $E_{x\_inc}(i\text{+}1/2, js)$ is subtracted to $E_x(i\text{+}1/2, js)$ for the advance of $H_z(i\text{+}1/2, js\text{+}1/2)$. In the corner, $E_y(is, js\text{-}1/2)$ can be advanced with (3), and $E_x(is\text{+}1/2, js)$ with the same modified equation as at the other $E_x(i\text{+}1/2, js)$ nodes. Concerning node $H_z(is\text{-}1/2, js\text{+}1/2)$ in the corner, the two derivatives on space of the FDTD advance involve only E_x and E_y in the scattered field region. From this, the regular FDTD equation can be used as it stands to advance the scattered field.

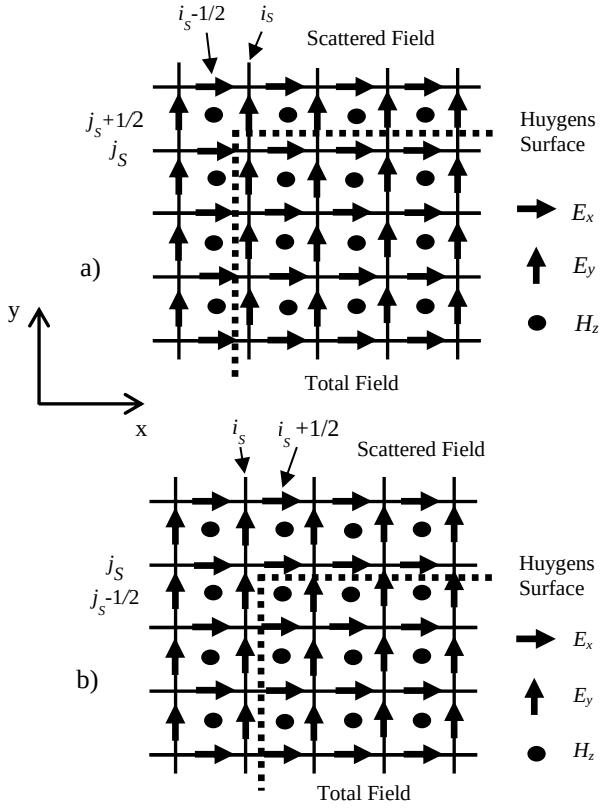

Fig. 2. Two implementations of the Total Field / Scattered Field method in a 2D domain.

Fig. 2b) shows another possible separation of the domain into two regions. Here the FDTD equations must be modified for the advance of $E_y(is, j+1/2)$ and $H_z(is+1/2, j+1/2)$ aside the vertical separation, and for the advance of $E_x(i+1/2, js)$ and $H_z(i+1/2, js-1/2)$ aside the horizontal separation. The modified equations can be derived in a similar manner as (3) and (5), that is by adding or subtracting the incident field in the transverse derivatives. A slight difference between the implementations in Figs. 2a) and 2b) is in the corners. In Fig. 2b), $E_y(is, js-1/2)$ and $E_x(is+1/2, js)$ can be advanced with the same modified equations as at any nodes $E_y(is, j+1/2)$ and $E_x(i+1/2, js)$. But the node $H_z(is+1/2, js-1/2)$ in the total field region is special. Here the two derivatives on space of the FDTD advance involve one E node in the scattered field region, so that the two derivatives must be modified. More explicitly, $E_{x\_inc}(is+1/2, js)$ must be added to $E_x(is+1/2, js)$, and $E_{y\_inc}(is, js-1/2)$ added to $E_y(is, js-1/2)$, in the FDTD advance of $H_z(is+1/2, js-1/2)$.

In summary, modifications of the FDTD equations permit the scattered and total fields to be advanced in time at the nodes on either side of the separation of the regions. The modifications concern the discrete derivatives perpendicular to the line separating the two regions. They consist either in adding the incident field to the FDTD scattered field or subtracting the incident field to the FDTD total field. In the literature, the modified FDTD equations are sometimes called the corrected FDTD equations since the addition or subtraction of the incident field appears as a correction to the regular equations.

The total field/scattered field method presented in the 2D case can be easily extended to the 3D case. Here the separation between the regions is a parallelepiped surface. The six faces are placed between FDTD planes, for instance a face perpendicular to x is placed between FDTD planes (E_x, H_y, H_z) and (E_y, E_z, H_x). The modifications of the FDTD equations for the advance of the nodes which are aside the six faces of the surface just consists in adding or subtracting the incident field to the discrete derivatives perpendicular to the separation of the region, in order that they are the desired derivatives of either the scattered or the total field. There is no special difficulty in the edges and corners. As in 2D (Fig. 2), depending on the choice of the location of the separation, the field components in the edge and corners can be advanced with the regular FDTD equation or with an equation where two derivatives on space are modified.

II-2. The interpretation of the Total field/ Scattered field method in terms of the Equivalence Theorem

In the above, the separation of the domain into two parts has been described in the discretized space of the FDTD method. The modifications to the FDTD equations come in a natural way and are rather trivial. However, the equations obtained in this context, such as (3) or (5), can also be viewed as the FDTD discretization of equations in the continuous space. More specifically, the FDTD equations can be viewed as resulting from the equivalence theorem. Indeed, the initial presentations of the method in the literature in [3], [4] were relying on the equivalence theorem, from which the FDTD equations were derived.

Let us consider an artificial surface S enclosing a volume V, and sources located outside V producing fields E_{inc} and H_{inc} on S. The equivalence theorem [4, 7] states that by removing the sources and impressing the following electric and magnetic current sheets on S

$$\vec{J}_S(S) = -\vec{n} \times \vec{H}_{inc}(S) \qquad \text{(6-a)}$$

$$\vec{K}_S(S) = \vec{n} \times \vec{E}_{inc}(S) \qquad \text{(6-a)}$$

there is no field outside S and the field within V is identical to the field (E_{inc}, H_{inc}) that was produced when the sources were present. In (6), n is the unit vector on S oriented outward and (E_{inc}, H_{inc}) is the incident field on S which is called the Huygens surface. By implementing S in the FDTD domain, the incident field can be generated in the interior of S while no field is produced outside it. If an object or any modification of the medium is introduced inside S, there is a scattered field added to the incident field inside S, i.e. a total field, while only the outgoing scattered field is present outside S.

The implementation of the equivalence theorem in the FDTD grid consists in enforcing J_S and K_S on a surface S, in general a parallelepiped enclosing the region of interest of the FDTD domain. This can be done by using the Maxwell equations in the presence of electric and magnetic current densities J and K

$$\varepsilon_0 \frac{\partial \vec{E}}{\partial t} = \vec{\nabla} \times \vec{H} - \vec{J} \qquad \text{(7-a)}$$

$$\mu_0 \frac{\partial \vec{H}}{\partial t} = -\vec{\nabla} \times \vec{E} - \vec{K} \qquad \text{(7-b)}$$

The current sheets J_S and K_S, which are zero in thickness, cannot be placed on the FDTD planes (or rows in 2D) where E or H nodes of the tangential components are located, because such components are discontinuous through J_S and K_S. From this, the Huygens surface must be somewhere between the FDTD planes, as the separation of scattered and total field regions in Figs. 1-2. Consider for instance the 2D case in Fig. 1 with an incident wave of components E_{x_inc}, E_{y_inc}, H_{z_inc} coming from the left-hand side. From (6) the current sheet J_S on the surface reduces to a component $J_{Sy}(j+1/2) = -H_{z\_inc}(is-1/2, j+1/2)$ where the value of H_{z_inc} has been chosen at the closest H_z node. For the advance of $E_y(is, j+1/2)$, the equation to be used is (7-a), which reduces to (2) with an additional term $-\Delta t/\varepsilon_0 J_y$. The current sheet (in A/m) J_{Sy} is equivalent to a current density (in A/m^2) $J_y = J_{Sy}/\Delta x$ flowing through the cell of width Δx. Equation (2) with the term $-\Delta t/\varepsilon_0 J_y$ then yields

$$E_y^{n+1}(is, j+1/2) = E_y^n(is, j+1/2) - \frac{\Delta t}{\varepsilon_0 \Delta x}\Big[H_z^{n+1/2}(is+1/2, j+1/2) - H_z^{n+1/2}(is-1/2, j+1/2)\Big] + \frac{\Delta t}{\varepsilon_0 \Delta x} H_{z\_inc}^{n+1/2}(is-1/2, j+1/2) \quad (8)$$

which is identical to (3). Similarly, from (6) we have $K_{Sz}(j+1/2) = -E_{y\_inc}(is, j+1/2)$, and using (4) with an additional term $\Delta t/\mu_0 K_z$, an equation identical to (5) is obtained.

The equivalent sources (6) placed as in Fig. 2 between FDTD rows or columns, also permit the modified FDTD equations of the total field/scattered field method to be obtained in the 2D corners.

In summary, the direct derivation of the equations in the discrete FDTD grid and the derivation of the equations from the continuous equations of the equivalence theorem yield the same advance of the FDTD fields in 2D and obviously in the 3D case as well. For the encoding of the method, reasoning in the discrete grid renders the implementation easier, especially in the edges and corners of the 3D case. It also permits easy implementation of the method in other media than in the vacuum considered in the above.

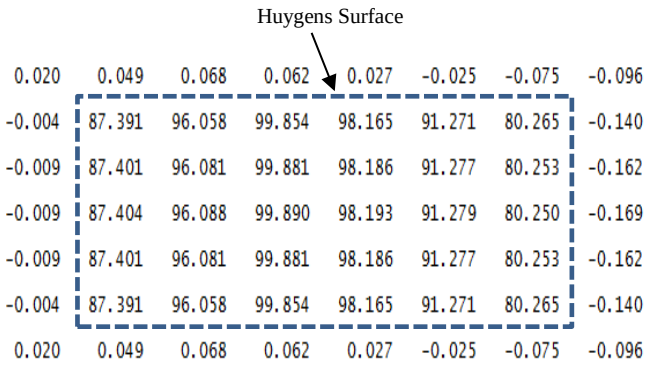

Fig. 3. E_y field component at the nodes of a 2D FDTD grid when an x-directed incident plane wave traverses a 5 x 5 total field region.

II-3. An experiment

An experiment is reported in Fig. 3. It demonstrates the effectiveness of the method to generating an incident wave within the Huygens surface while no field is produced outside it, in theory. The incident wave is a Gaussian pulse E_y=100 exp $[(t-5\tau)^2/\tau^2]$ with $\tau = 10\ \Delta t$. The problem is 2D with the implementation in Fig. 2a. The FDTD steps are $\Delta x = \Delta y = 5$ cm and $\Delta t = 0.1$ ns, the wave is incident from the left, in the x direction, with polarization (E_{inc_y}, H_{inc_z}). The size of the Huygens surface is 5 x 5 FDTD cells. Fig. 3 is a snapshot of the E_y component at the E_y nodes, at the time where the peak value of the pulse is within the surface. As can be observed, the incident wave is well reproduced within the surface, while outside it the field is quite small. However, this field is not exactly zero, it is called the leakage of the Huygens surface. It is due to the dispersion of the FDTD method and then mainly depends on the ratio of the wavelength to the FDTD space step. Here the leakage is of the order of 1/1000 the peak value, it would be either larger with a shorter pulse or smaller with a larger pulse. Techniques to reduce this spurious leakage have been developed and are the matter of the next section.

II-4. Generation of the incident wave

The incident field is by hypothesis a data of the problem. For an incident plane wave, it can be easily computed at any time and at the nodes where it must be added or subtracted to the field present in the grid. The calculation must account for the time and the delay of propagation to the considered node. This can be done in a trivial manner by an analytical calculation. However, to reduce the computational time devoted to the calculation at all the nodes of the Huygens surface and at every FDTD time steps, which may be large if the waveform is complicated, a method describe in [8] consists in calculating the incident waves along a line parallel to the direction of propagation, at locations separated with a certain space step Δ_p. The incident wave at the desired nodes of the Huygens surface can then be obtained by a simple interpolation of the 1D pre-calculated field. The 1D pre-calculation can be performed analytically, but it can also be performed by means of a 1D FDTD calculation [8]. The latter method has some advantages. In particular, by choosing the time and space steps of the 1D calculation equal to those of the 3D domain, it permits the spurious effect of the FDTD dispersion to be cancelled when the propagation is parallel to an axis of coordinate. This method was at the origin of the auxiliary equation methods that were later developed to reduce the effect of dispersion at any incidence angle.

III. Reduction of the Spurious Effect of Dispersion

The methodology for the discrete plane wave (DPW) source that is utilized in [8] is rooted in a realization that a plane wave is inherently a (spatially) one-dimensional structure. That is, the fields in a plane wave can be completely described by how they vary spatially in terms of a single spatial variable r which describes distance in the direction of propagation. We do this all the time when we assume a phasor form and describe the fields in a plane wave as $\vec{E}(\vec{r}, t) = \hat{E}_0 e^{j(\omega t - \vec{k}\cdot\vec{r})} = \hat{E}_0 e^{j(\omega t - kr)}$. We can choose an arbitrary reference point, so in this case we have assumed the wavevector and position vector are parallel. Although the fields in the plane wave are spatially three-dimensional, only one dimension is necessary because the fields in any plane perpendicular to the direction of propagation are (by definition) identical to each other.

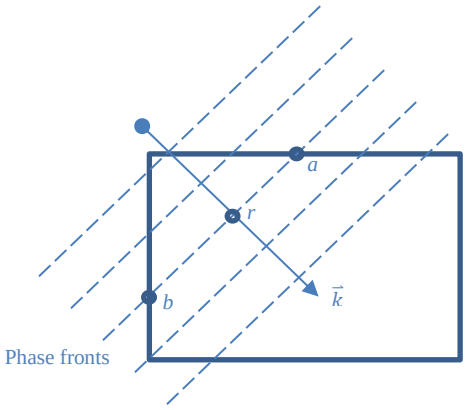

Fig. 4. Plane wave propagating in a direction parallel to wave vector $\vec{k}$. Planes of equal phase are indicated by dashed lines. The plane wave can be represented by a 1D object (the arrow), with any point on the object referenced by position *r*.

This idea can be visualized in Fig. 4, where the plane wave is shown propagating in a direction parallel to the wave vector

$$\vec{k} = (k_x, k_y, k_z) = k\vec{p}$$

where

$$\vec{p} = (p_x, p_y, p_z) = (\sin\theta\cos\varphi\,, \sin\theta\sin\varphi\,, \cos\theta)$$

is a unit vector which we will call the *projection vector* which defines the direction of propagation. Note that the fields at points *a* and *b* are identical to each other (they are on the same phase front), and are equal to the field at a distance *r* in the 1D description of the plane wave. In fact, the values of the plane wave fields at *any* point in the 3D space – for instance, the points on the bounding box in Fig. 4 – can be found by a projection onto the 1D line which describes the plane wave. This is true for fields in both continuous and discrete domains.

In [8], this concept is used by assuming an auxiliary 1D grid (the grid in spatial variable *r*, with spacing Δ_r) on which the incident plane wave field is propagating. Using Fig.4, consider that the points *a* and *b* lie on the Huygens surface, and we require the incident fields there. These are found by projecting those points onto the 1D auxiliary grid, where the geometry dictates the values of the fields used.

However, there are two fundamental problems with the implementation in [8], namely (i) points on the Huygens surface are not directly projected onto points in the 1D grid necessarily (they often lie in between two field points), thus requiring interpolation; and (ii) the numerical dispersion properties of the 1D grid are different from those in the 3D grid. The combination of these two issues introduces errors in the plane wave source, which manifests as non-physical leakage fields in the scattered field region, which can be at the level of -30 to -40dB of the incident field. This essentially sets the dynamic range of the simulation, and thus limits its applicability. Subsequent authors have suggested using signal processing techniques to reduce this error to the level of -70dB [9-11], but this can still be too high for some simulation requirements.

Fundamentally there should be no reason to require interpolation, because at least conceptually we should be able to map every 3D field point to a point in the 1D domain. Furthermore if we start that mapping from the discrete 3D FDTD Yee grid, then we should have exact mapping *and* identical dispersion properties. The following two subsections will outline how this concept can be implemented, the first being in the frequency-domain, and the second being in the time-domain.

III-1. Analytic Field Propagator (AFP) Method

The Analytic Field Propagator (AFP) method is outlined by Schneider in [12] and is based on the idea that – in the frequency domain – the fields in a plane wave at any location $\vec{x} = (m_x\Delta_x, m_y\Delta_y, m_z\Delta_z)$ - where m_i are used to indicate the geometric position of a field in the Yee grid, but are not necessarily integers - can be found through a phase shift of the fields at some reference location. Consider the phasor description of electric and magnetic fields for a plane wave in an FDTD grid, given by

$$\widehat{\boldsymbol{E}} = \widehat{\boldsymbol{E}}_0 e^{j\left(\omega n\Delta_t - \vec{k}\cdot\vec{x}\right)} = \widehat{\boldsymbol{E}}_0 e^{j(\omega n\Delta_t - k_x m_x\Delta_x - k_y m_y\Delta_y - k_z m_z\Delta_z)}$$
$$\widehat{\boldsymbol{H}} = \widehat{\boldsymbol{H}}_0 e^{j\left(\omega n\Delta_t - \vec{k}\cdot\vec{x}\right)} = \widehat{\boldsymbol{H}}_0 e^{j(\omega n\Delta_t - k_x m_x\Delta_x - k_y m_y\Delta_y - k_z m_z\Delta_z)}$$

Assuming these solutions for the fields in the FDTD grid, it was shown in [12] how the update equations can be written in terms of the variables

$$K_i = \frac{2}{\Delta_i}\sin\left(\frac{k_i\Delta_i}{2}\right)$$
$$\Omega = \frac{2}{\Delta_t}\sin\left(\frac{\omega\Delta_t}{2}\right)$$

which also allows for the 3D FDTD dispersion equation to be written as

$$\mu\varepsilon\Omega^2 = K_x^2 + K_y^2 + K_z^2$$

These variables completely capture the temporal and spatial frequency (spectral) characteristics of the fields.

Now consider that the incident plane wave is to have a time series *f*(*t*) at some reference location $(m_{x,ref}, m_{y,ref}, m_{z,ref})$. Then e.g. the electric field E_z at any other node in the grid is given, in the frequency domain, as

$$\hat{E}_z(m_x, m_y, m_z) = P_{\vec{x}}(m_{x,ref}, m_{y,ref}, m_{z,ref})\mathcal{F}(f)$$

where

$$P_{\vec{x}}(m_{x,ref}, m_{y,ref}, m_{z,ref}) = exp\{-j[k_x\Delta_x(m_x - m_{x,ref}) + k_y\Delta_y(m_y - m_{y,ref}) + k_z\Delta_z(m_z - m_{z,ref})]\}$$

is the complex-valued propagator which implements the phase-shift, and $\mathcal{F}(f)$ is the discrete Fourier transform of the time series for the reference field. In the time-domain the field is given by the inverse Fourier transform $E_z(m_x, m_y, m_z) = \mathcal{F}^{-1}\left(P_{\boldsymbol{m}}(m_{x,ref}, m_{y,ref}, m_{z,ref})\mathcal{F}(f)\right)$.

Using the spectral variables, the time-domain magnetic fields can then be found as e.g.

$$H_x = \mathcal{F}^{-1}\left\{\frac{K_y}{\mu\Omega}\widehat{E}_z\right\}$$

$$H_y = \mathcal{F}^{-1}\left\{-\frac{K_x}{\mu\Omega}\widehat{E}_z\right\}$$

Equations for arbitrary 3D waves and polarizations can be found by extension of these examples, and by including the polarization terms as outlined in [12].

Because the AFP method is derived *directly* from the 3D FDTD dispersion equation, there is a perfect match between the source fields and the target (3D) domain; the source is consistent with the 3D FDTD update equations. Furthermore, there is no need for interpolation as fields at *any* location in space can be determined directly. As a result of this, the examples presented in [12] show scattered field leakage errors at the level of -100 to -180dB, or essentially at machine precision levels (depending on the accuracy of the discrete Fourier transforms).

Because the AFP method operates in the frequency domain, one of the drawbacks in its utilization with the TF/SF method is that all of the required source fields for the Huygens' surface must be calculated in pre-processing (via the inverse discrete Fourier transform) and stored for utilization in runtime. This is still relatively little storage compared to the 3D field arrays (a 2D surface of fields vs. 3D volume), but the entire time sequence for all those 2D fields must be stored. In the following section we discuss a method which overcomes this drawback by implementing the idea directly in the time-domain.

III-2. Discrete Plane Wave (DPW) Method

We start again with the concept that a plane wave is inherently a 1D structure, and that all field values in 3D space $\vec{x} = (i\Delta_x, j\Delta_y, k\Delta_z)$ for the plane wave can be related back to this 1D structure through projection. The 1D plane wave structure is geometrically envisaged as a line lying in a direction defined by the projection vector $\vec{p}$, and points on the line are referred to by the variable *r*. The projections of the 3D fields to this 1D structure are thus defined by

$$r = \vec{p}\cdot\vec{x} = p_x i\Delta_x + p_y j\Delta_y + p_x k\Delta_z$$

where, again, i, j, k do not necessarily have to be integers. The DPW method, introduced in [13] by Tan and Potter, is based on this building block, and allows us to construct a perfect plane wave source directly in the time domain. The premise of the DPW method is to start with the original 3D FDTD update equations, and convert them to (six coupled) 1D update equations by utilizing the projection operation above. These six equations should then allow the 'perfect' propagation of a plane wave, in the sense that they exactly replicate how a plane wave would propagate in the 3D grid, with no dispersion mismatch artifacts, nor interpolation.

As an example, take the 3D update equation for the *x*-component of the electric field

$$\begin{aligned}E_x^{n+\frac{1}{2}}&\left(i, j+\tfrac{1}{2}, k+\tfrac{1}{2}\right)\\ &= E_x^{n-\frac{1}{2}}\left(i, j+\tfrac{1}{2}, k+\tfrac{1}{2}\right)\\ &+\frac{\Delta_t}{\varepsilon\Delta_y}\left[H_z^n\left(i, j+1, k+\tfrac{1}{2}\right) - H_z^n\left(i, j, k+\tfrac{1}{2}\right)\right]\\ &+\frac{\Delta_t}{\varepsilon\Delta_z}\left[H_y^n\left(i, j+\tfrac{1}{2}, k\right) - H_y^n\left(i, j+\tfrac{1}{2}, k+1\right)\right]\end{aligned}$$

Using the projection operation above, we can rewrite this equation for the 1D grid in *r*, finding

$$\begin{aligned}E_x^{n+\frac{1}{2}}&\left(r = p_x i\Delta_x + p_y\left(j+\tfrac{1}{2}\right)\Delta_y + p_x\left(k+\tfrac{1}{2}\right)\Delta_z\right)\\ &= E_x^{n-\frac{1}{2}}\left(p_x i\Delta_x + p_y\left(j+\tfrac{1}{2}\right)\Delta_y\right.\\ &\left.+ p_x\left(k+\tfrac{1}{2}\right)\Delta_z\right)\\ &+\frac{\Delta_t}{\varepsilon\Delta_y}\left[H_z^n\left(p_x i\Delta_x + p_y(j+1)\Delta_y\right.\right.\\ &\left.+ p_x\left(k+\tfrac{1}{2}\right)\Delta_z\right)\\ &\left.- H_z^n\left(p_x i\Delta_x + p_y j\Delta_y + p_x\left(k+\tfrac{1}{2}\right)\Delta_z\right)\right]\\ &+\frac{\Delta_t}{\varepsilon\Delta_z}\left[H_y^n\left(p_x i\Delta_x + p_y\left(j+\tfrac{1}{2}\right)\Delta_y + p_x k\Delta_z\right)\right.\\ &- H_y^n\left(p_x i\Delta_x + p_y\left(j+\tfrac{1}{2}\right)\Delta_y\right.\\ &\left.\left.+ p_x(k+1)\Delta_z\right)\right]\end{aligned}$$

After following the same procedure for the remaining five update equations, one has a set of six coupled update equations which relates fields components spatially through a *single* variable *r*; however, the position in that variable still depends on three indices *i*, *j*, *k* and so the complexity has (apparently) not been reduced to 1D yet.

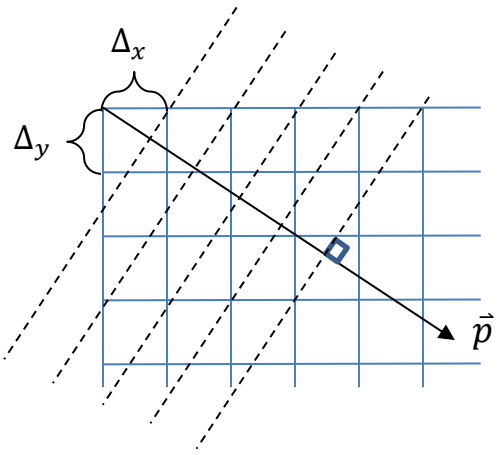

Fig. 5. Plane wave propagating in direction defined by projection vector $\vec{p}$, with dotted lines indicating phase fronts. Phase fronts are restricted to orientations defined by integer ratios of grid cells; in this case $m_x = 3$ and $m_y = 2$.

Consider that a plane wave – by definition – requires that fields with equal values share a common phase front which is perpendicular to the direction of propagation. For the 3D discrete space upon which FDTD is built, we can introduce a restriction such that the phase front must pass through at least two field points lying at permitted FDTD field locations. It turns out that this is equivalent to restriction of the allowed

angles of propagation such that the projection vector satisfies the following

$$p_i \Delta_i = m_i \Delta_r, \quad i = x, y, z$$

where m_i must be integers, and Δ_r is uniform discrete spacing on the *r*-grids (six: one for each field component) that is yet to be determined. This is demonstrated in Fig. 5 in two dimensions as an example. Note the wave is restricted to travelling in directions defined by integer ratios of grid cells, but effectively any angle can be represented by choosing the integers appropriately. The azimuthal and polar angles permitted with these restrictions can be found as

$$\tan\varphi = \frac{p_y}{p_x} = \frac{m_y \Delta_x}{m_x \Delta_y}$$

$$\tan\theta = \frac{\sqrt{p_x^2 + p_y^2}}{p_z} = \frac{\sqrt{\left(\frac{m_x}{\Delta_x}\right)^2 + \left(\frac{m_y}{\Delta_y}\right)^2}}{\frac{m_z}{\Delta_z}}$$

With this restriction, the values of *r* now become

$$r = \left(m_x i + m_y j + m_z k\right)\Delta_r = i_r \Delta_r$$

where $i_r = m_x i + m_y j + m_z k$ indexes the gridpoint on the (now uniformly) sampled *r*-grid, thus transforming the field update equations to

$$\begin{aligned} E_x^{n+\frac{1}{2}}\left(i_r + \tfrac{m_y}{2} + \tfrac{m_z}{2}\right) = {} & E_x^{n-\frac{1}{2}}\left(i_r + \tfrac{m_y}{2} + \tfrac{m_z}{2}\right) + \\ & \tfrac{\Delta_t}{\varepsilon \Delta_y}\left[H_z^n\left(i_r + m_y + \tfrac{m_z}{2}\right) - H_z^n\left(i_r + \tfrac{m_z}{2}\right)\right] \\ & + \tfrac{\Delta_t}{\varepsilon \Delta_z}\left[H_y^n\left(i_r + \tfrac{m_y}{2}\right) - H_y^n\left(i_r + \tfrac{m_y}{2} + m_z\right)\right] \quad (9) \end{aligned}$$

and likewise for the other five. The half-integer values only show in the updates because they represent actual physical (geometric) locations from the 3D grid, but from an indexing perspective in programming they are superfluous. Rather it is the difference in location of field components that matters: for instance, in (9) the indexing difference between the two H_z components is m_y. Therein lies the difference between the 3D update equations and the 1D update equations: in the former, finite differences are with fields that differ in index by 1, but in the latter they are with fields that differ in index by m_i (depending on the direction of the derivative).

Some other nuances of the method are outlined in [13] and [14, Chap. 3], such as accounting for polarization, time-series source fields for the 1D grids and boundary conditions, but in summary the following steps are needed to implement the method:

- Identify the angle required for the incident plane wave and choose m_i appropriately
- Establish six incident plane wave field arrays, with time-series source fields and boundary conditions
- During run-time: perform updates on regular 3D FDTD equations;
- During run-time: perform updates on 1D source equations; and
- During run-time: generate required incident field correction terms for Huygens' surface through direct mapping

The computational complexity of this method is only $O([m_x + m_y + m_z]N)$, and unlike the AFP method no pre-processing and storage of time-series is required.

Several examples of the DPW in practice at different angles can be found in [13] and [14] which demonstrate the efficacy of the method. In all cases, leakage in the scattered-field region for empty total-field regions is at the level of machine precision (-300dB at double-precision). This remarkable level is achievable because the numerical dispersion is perfectly matched, and there is no interpolation necessary because every 3D field component is mapped to a location on the 1D propagator grids. This level of error is achievable regardless of the propagation angle, grid cell ratio, and even the frequency content of the time signal. In one experiment, a square pulse train was utilized as the time source signal and - although this was severely distorted by numerical dispersion in propagation – there was still no leakage into the scattered-field region.

Effectively what the DPW methodology does is provide a source that is perfectly calibrated to the 3D computational domain, effectively eliminating any mismatch error between the 1D source domain and the 3D simulation domain. This is of practical importance for researchers that need TF/SF simulations with high dynamic range e.g. for studies of objects with very low RCS, microwave breast tumor detection simulations where received scattered signals are very low due to high attenuation, etc.

IV. Extensions of the TF/SF Method

The TF/SF method was introduced and remains mainly used for the generation of an incident plane wave in FDTD domains containing objects situated in background medium which is vacuum. However, it has been also used in other media and in other contexts. This is reviewed in the following sections.

IV-1. Use of the TF/SF method in other media

The equivalence theorem is valid in a vacuum as well as in any other media [7], and in particular in lossy media and in dispersive media where the conductivity and the permittivity depend on frequency. From this, the TF/SF method can be extended to any media. This is also evident by considering a total field region and a scattered field region in the discretized FDTD domain. As in a vacuum, implementing the Huygens surface just consists in either adding or subtracting the incident field to the derivatives that involve one node in the scattered field and one node in the total field. As an example, if the vacuum in Fig. 1 is replaced with a lossy medium of permeability ε_r and conductivity σ, the FDTD equation (3) is replaced with

$$\begin{aligned} E_y^{n+1}(is, j+1/2) = {} & A E_y^n(is, j+1/2) - \frac{\Delta t}{\varepsilon_r \varepsilon_0 \Delta x} B\Big[H_z^{n+1/2}(is+1/2, j+1/2) \\ & - \left\{H_z^{n+1/2}(is-1/2, j+1/2) + H_{z\_inc}^{n+1/2}(is-1/2, j+1/2)\right\}\Big] \quad (10) \end{aligned}$$

where

$$A = e^{-\frac{\sigma \Delta t}{\varepsilon_r \varepsilon_0}} \qquad B = \frac{(1-A)}{\sigma \Delta t}$$

In the literature, there are several papers reporting use of the TF/SF method in dielectric or lossy media [15-20], in Debye media [21], and in artificial absorbing layers [22-23]. In addition to the losses, the media are layered in [18-19] and layered and anisotropic in [20].

IV-1-1. *TF/SF method in dielectric and lossy media*

The first papers reporting use of the TF/SF method in other media than in a vacuum are [15-16]. In [15] the space is composed of two parts, more precisely with a vacuum situated above a ground which may be a dielectric or a lossy medium (Fig. 6). The incident wave comes from the vacuum and strikes the vacuum-ground interface. The incident field to be applied on the Huygens surface above the interface is then the addition of the incident plane wave with the plane wave reflected from the interface, while below the interface the incident wave is the wave transmitted through the interface. In [15], these incident waves are computed analytically using the Fresnel coefficients of reflection and transmission at the interface. The results in [15] demonstrate the effectiveness of the TF/SF method in this relatively complex problem involving an interface. In [16], part of the Huygens surface also is in a dielectric slab, and the incident field is computed by means of a FDTD auxiliary equation. Later, [17] addressed a similar problem with the Huygens surface extended into a lossy ground.

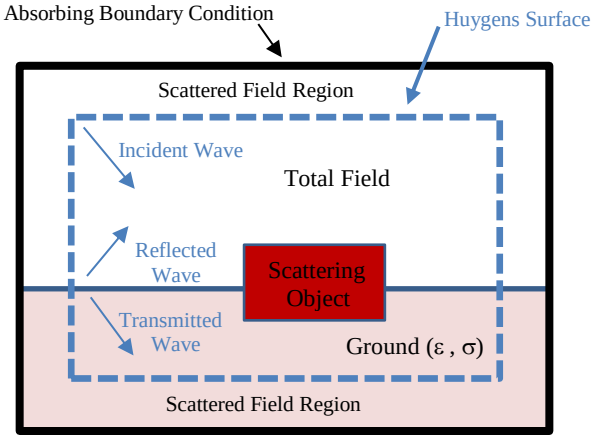

Fig. 6. Huygens surface in part in vacuum and in part in a dielectric or lossy Ground.

IV-1-2. *TF/SF in layered media*

The media addressed in [18-19] are layered, with dielectric or lossy media separated with interfaces. Again, the implementation of the Huygens surface is like in a vacuum, with the addition or subtraction of the incident field at nodes contiguous to the surface. In [19] the incident plane wave propagates in an arbitrary direction with respect with the interfaces. The geometry is shown in Fig. 7. Most of [19] is devoted to the description of the method used to compute the incident field on the Huygens surface. This field is the wave in the absence of any scattering structure, but in the presence of the interfaces between the media.

In theory, the incident wave could be computed by using analytical formulae in conjunction with Fourier transforms to deal with the lossy media. But in [19], it is computed by means of an auxiliary 1D FDTD grid, which permits savings of computational time. The propagation of the incident wave is 1D because the problem is invariant in the direction *y* perpendicular to the plane of incidence, which means $\delta/\delta y=0$, and because the phase matching at the interfaces permits another derivative on space to be connected to the derivative on time by the relationship

$$\frac{\partial}{\partial x} = \frac{\sin\theta}{c}\frac{\partial}{\partial t} \tag{11}$$

where θ is the incidence angle and *x* is the direction belonging to the plane of incidence and parallel to the interfaces. Equation (11) and $\delta/\delta y=0$ permit the Maxwell equations governing the incident wave to depend only on the *z* direction perpendicular to the interfaces. This 1D auxiliary equation is in the same form as the equation of transmission lines, it can be solved by the FDTD method to obtain the incident wave at some discrete time and space steps. Interpolation then provides the field to be injected on the 3D Huygens surface.

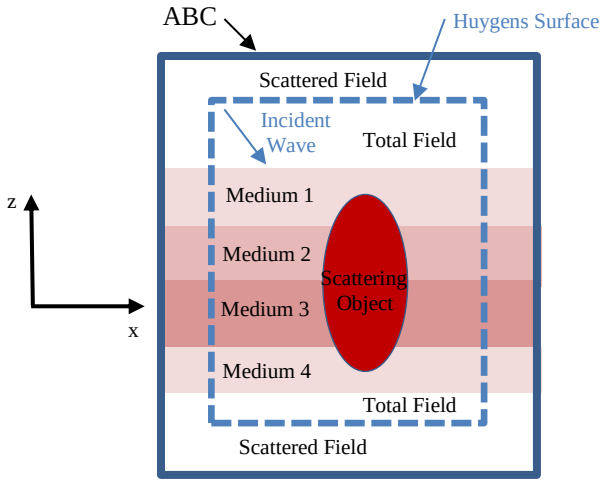

Fig. 7. Huygens surface in a layered medium. Cut in the plane of incidence.

The results in [19] shows that the method allows the incident wave to be well reproduced within the Huygens surface, as illustrated with a 3-layer dielectric medium where the difference between the theoretical incident wave and the FDTD field within the Huygens surface is only 0.7 % of the peak value.

IV-1-3. *TF/SF in anisotropic layered media*

The method presented in [20] for the generation of an incident wave in a 2D anisotropic layered medium is basically the same as in [19], in particular it relies on (11) to reduce the propagation of the incident wave to a 1D problem. It mainly differs with the use of 1D split field equations where the *D* vector is split into two subcomponents, as it is done in the split PML absorbing boundary condition. This is because the TE

and TM polarizations of the incident wave are coupled in the anisotropic media, conversely to the case in [19] where they are decoupled. Numerical experiments in [20] illustrates the effectiveness of the method in such layered and anisotropic media. The error is evaluated in terms of the leakage outside the Huygens surface. For the reported experiments, the leakage is lower than -40 dB with respect to the peak value of the incident wave.

IV-1-4. *TF/SF in Debye media*

Debye media are dispersive media that can be used for modeling human tissues. In such media the permittivity is complex and frequency dependent. More precisely

$$\varepsilon_r(\omega) = \varepsilon_\infty + \frac{\varepsilon_S - \varepsilon_\infty}{1 + j\omega\tau} + \frac{\sigma}{j\,\varepsilon_0\omega} \qquad (12)$$

where ε_S and ε_∞ are the static and optical relative permittivities, σ is the conductivity, and τ the relaxation time. Permittivity (12) is equivalent to the following time domain relationship connecting the D and E vectors in the medium

$$\tau\frac{\partial^2 \boldsymbol{D}}{\partial t^2} + \frac{\partial \boldsymbol{D}}{\partial t} = \varepsilon_0\varepsilon_\infty\tau\frac{\partial^2 \boldsymbol{E}}{\partial t^2} + (\varepsilon_0\varepsilon_S + \sigma\tau)\frac{\partial \boldsymbol{E}}{\partial t} + \sigma\,\boldsymbol{E} \qquad (13)$$

The FDTD scheme in this medium [21] consists in advancing the H field with the Maxwell-Ampere equation, as in a vacuum, and advancing the D vector using the discretized form of the Maxwell-Faraday equation

$$\frac{\partial \vec{D}}{\partial t} = \vec{\nabla} \times \vec{H} \qquad (14)$$

The advanced E field is then obtained from the advanced D by means of the discretized form of (13).

As in a vacuum, the interface between the scattered and total field regions, i.e. the Huygens surface, is accounted for in the equation of Maxwell-Faraday, used here for the advance of D. The incident field H_{inc} is added or subtracted to the FDTD H field to render the derivatives on space either total or scattered derivatives. For instance, if the domain in Fig. 1 is filled with a Debye medium, the advance of D_y which is computed at the same nodes as E_y, reads at $i = is$

$$D_y^{n+1}(is, j+1/2) = D_y^n(is, j+1/2) - \frac{\Delta t}{\Delta x}\Big[H_z^{n+1/2}(is+1/2, j+1/2) - \left\{H_z^{n+1/2}(is-1/2, j+1/2) + H_{z\_inc}^{n+1/2}(is-1/2, j+1/2)\right\}\Big]$$

which is nothing but (3) with D_y in place of $\varepsilon_0 E_y$. Note the auxiliary equation (13) is a local equation, without spatial derivatives, so that its discrete form does not need any modification near the Huygens surface.

The advance of the H field is the same as in a vacuum, for instance (5) is valid in a Debye medium.

The results in Fig. 8 show the E field generated within a 100x100x100 Huygens surface in a computational domain filled with Skin tissue. The incident wave is a Gaussian pulse of magnitude 100 as it hits the Huygens surface. As the wave propagates in the total field region the high frequencies are more absorbed than the low frequencies, the peak value decreases and the pulse is enlarged. The field in the FDTD domain agrees well with the theoretical propagation in the medium.

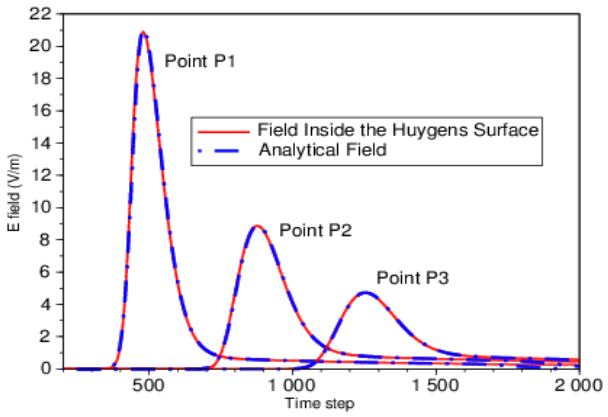

Fig. 8. *E* field within a 100x100x100-cell Huygens surface at three points P1, P2, P3, located 33, 66, 99 cells from the front side. The FDTD domain is filled with a Debye medium (Skin tissue). The space step is 1 mm and the time step 2 ps.

In [21] the incident field is computed either analytically or using an auxiliary equation which cancels the spurious effect of the dispersion when the incident wave propagates in direction of an axis of coordinates. The leakage out of the Huygens surface depends on more parameters than in a vacuum, because of the dispersive nature of the Debye media. Leakage below -40 dB can be easily obtained [21] even using the analytical incident field. Notice that the leakage in Debye media is probably less critical than in vacuum, because it is also absorbed by the medium.

IV-1-5. *TF/SF in artificial absorbing media*

The TF/SF method has been used in [22] in a matched medium where electric and magnetic losses are present in order that the impedance is the same as that in a vacuum. Use of this medium with small losses in place of a vacuum in the inner domain allows the low frequency numerical reflection from the FDTD PML to be reduced. To implement the Huygens surface, the modifications of the FDTD equations are again as in other media, i.e. the derivatives transverse to the Huygens surface are corrected with the incident field. For instance, the modified E field equation in the medium is (10) in the case of Fig. 1.

In [23], the TF/SF method is implemented, in part, in the PML absorbing boundary condition (Fig. 9). Both the scattering object and the Huygens surface penetrate into the PML. This permits the computation of the field scattered by such infinite scatterers as dielectric or PEC wedges. The incident field added or subtracted in the derivatives on space of the PML equations is the field present in the PML when a plane wave traverses the inner vacuum. That is the field of the desired plane wave either attenuated or amplified, depending on the situation of the PML with respect with the direction of propagation of the wave (amplified at the Huygens surface parts situated in the wall PMLs from which the incident plane wave enter the inner domain). When dealing with infinite scatterers, the extension of the Huygens surface into the PML, called the generalized TF/SF method in [23], allows the computational burden to be considerably reduced in comparison with calculations using time-gating procedures [23].

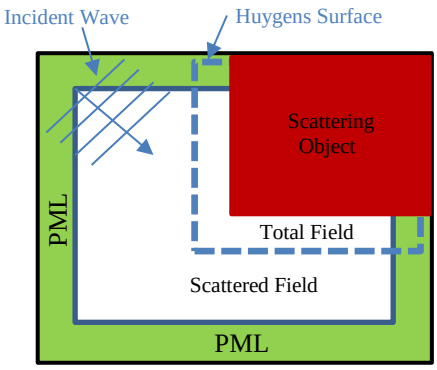

Fig. 9. The Huygens surface partially within the PML for the calculation of scattering by an infinite 2D right-angle dielectric wedge.

IV-2. Use of the Huygens method to generate the far field radiation of an antenna

The TF/SF method is used in [24] to generate the field radiated by an antenna. In this paper the FDTD method is applied to the computation of the propagation of very low frequency (VLF) radiowaves in the Earth-Ionosphere waveguide. The calculation is performed within a 2D domain (Fig. 10) which assumes that the problem is of symmetry of revolution around a vertical axis. From this, the field radiated by the antenna also must be of symmetry of revolution. With a dipole antenna, the condition holds only with a vertical dipole. For any other orientation, the radiated field is not uniform in the direction transverse to the 2D domain, it has non zero derivatives in the direction perpendicular to the 2D domain.

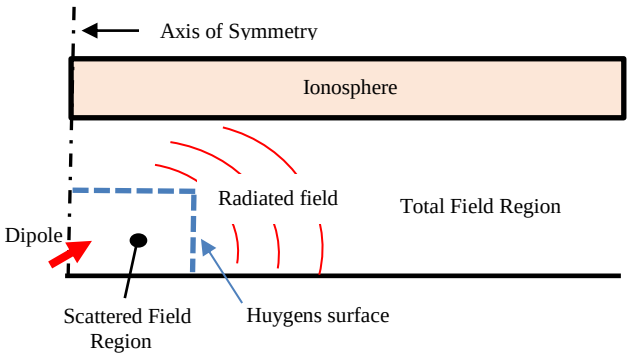

Fig. 10. Generation of the far field of a dipole antenna radiating in the Earth-Ionosphere 2D waveguide.

By using the formulae that give the radiated components of a short dipole, it can be shown that the transverse derivatives of the radiated field are composed with terms decreasing as $1/r^2$ and $1/r^3$, where r is the distance from the dipole. Since on the other hand the magnitude of the field is composed with terms decreasing as $1/r$, $1/r^2$, $1/r^3$, the derivatives in the transverse direction become negligible in the far field region where the term $1/r$ is preponderant. In other words, the problem is 3D in the vicinity of the dipole and becomes 2D some distance away. The radiation of any dipole, and more generally any antenna, can then be propagated in the 2D FDTD domain, provided that the field is generated out of the near field region. This can be achieved by means of a Huygens surface that replaces the source. This is what is done in [24], illustrated in Fig. 10. The incident field at the FDTD nodes where it is needed is computed with the analytical formulae of the short dipole antenna. Numerical experiments showed that the Huygens surface can be placed about two wavelengths from the dipole.

In summary, the Huygens surface can be used to replace radiating structures when they cannot be implemented in a direct manner. This is the case in [24] because of the solution in a 2D domain, but may also be the case in other contexts, for instance when the discretization is not fine enough to be able to accurately model the antenna.

IV-3. Use of the TF/SF method in subgridding techniques

Subgridding methods consist of coupling several FDTD grids in order that the discretization can be finer in some parts of the computational domain. In most cases, the grids, each one with its own space step, are connected in a direct manner. Conversely, with the methods reviewed in the following the grids are not connected, the coupling of the electromagnetic field is realized by means of Huygens surfaces. Two-way connections are realized in the exact Huygens subgridding method, and one-way connections in the approximate dual grid method which is simpler and well suited to some practical problems.

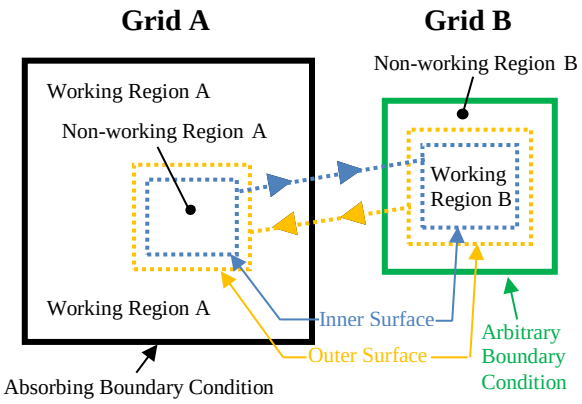

Fig. 11. The Huygens Subgridding method. Two FDTD domains are connected by means of two Huygens surfaces, the Inner surface IS and the Outer surface OS.

IV-3-1. *The Huygens Subgriding (HSG) method*

With the HSG method [25], the FDTD grids are connected by means of two Huygens surfaces. This is summarized in Fig. 11 for the case of a main grid A and a subgrid B. The Inner surface (IS) radiates the field from grid A into grid B, and the outer surface (OS) radiates the field from grid B into grid A.

The incident fields of Huygens surfaces IS and OS are the fields present at the same physical location in the other grid. The FDTD advances are run simultaneously, with *ns* substeps in the subgrid during one main step, where *ns* is the ratio of the space and time steps of the grids. In other words, the incident fields of IS and OS are not known a priori, they are provided on the fly by the other grid. It is shown in [25] and [28] that in continuous spaces the set of two grids is equivalent to a single domain composed with the working regions and the space between OS and IS (Fig. 11). This means that there is no approximation, all the interactions between sources and

objects placed in the working regions of the two grids are accounted for in an exact manner.

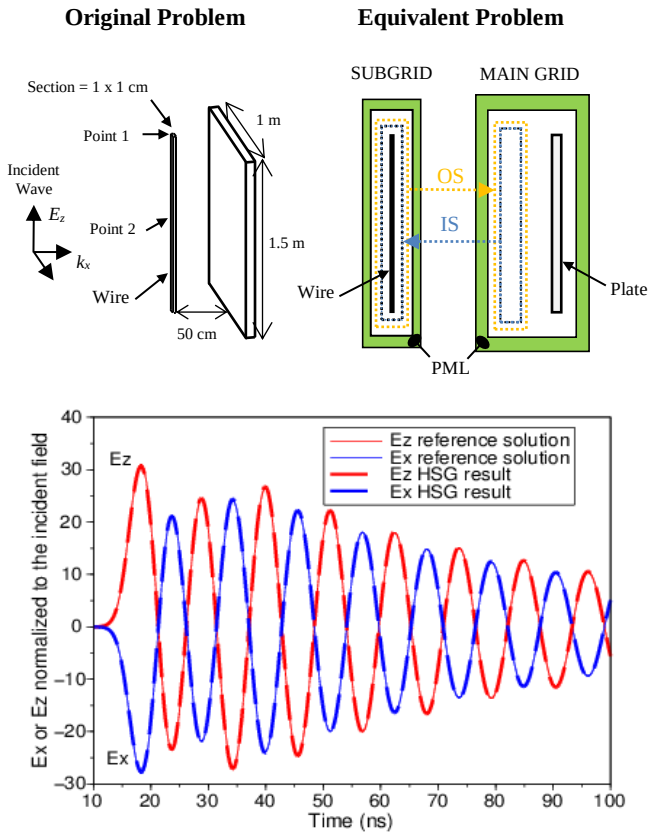

Fig. 12. Field on a wire stricken by an incident wave, with a plate 50 cm behind the wire. The upper part shows the physical problem and its equivalent one where the wire is in the subgrid and the plate in the main grid. The lower part compares the *E* field at the end of the wire (point 1) with reference solutions computed with a fine grid in the whole FDTD domain. The coarse step is 5 cm, the fine step 1 cm, the incident wave is a Gaussian pulse of width 2.5 ns.

Fig. 12 shows a 3D experiment where a HSG calculation is compared with a reference solution obtained using a single fine grid. The upper part shows the original physical problem and its equivalent problem composed with two grids connected by the IS and the OS. The ratio of steps is *ns* = 5. In this experiment, the energy oscillates between the wire and the plate, it passes many times through IS and OS. The agreement of the HSG results with the reference solutions is excellent.

The HSG permits arbitrarily high ratios of space steps to be used. Its sole drawback is the presence of a late time instability in some cases, a drawback it shares with some other subgridding techniques. It can be used in other media than vacuum, for example in Debye media [27, 29].

IV-3-2. *The Dual Grid (DG) method*

Huygens surfaces are also used to connect FDTD grids in the method described in [30-32]. There, only one Huygens surface is used to connect two grids. In continuous space, the method is exact, but with some restrictions on the locations of the sources and the desired results. And the FDTD implementation relies on some approximations. However, the method is well suited to some practical problems where the assumptions hold. This is the case for the problem addressed in [31] which consists of computing the signal received at a location on the human body from an antenna also placed on the body.

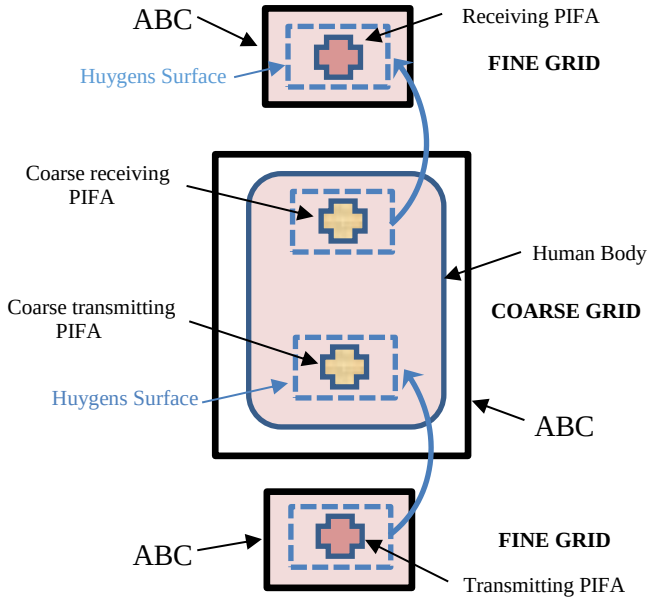

Fig. 13. Three FDTD grids connected by Huygens surfaces for the calculation of the signal transmitted between two PIFAs located on a human body phantom.

In [31], three FDTD domains are used. The first one, the lower in Fig. 13, is a fine grid with space step fine enough to accurately model a radiating planar inverted-F antenna (PIFA). The radiated field is enforced in the second grid by means of a Huygens surface. This second grid is large and coarse and covers the whole problem of interest, including a coarse model of the PIFA, a simple model of the human body, and a coarse model of the receiving antenna which is also a PIFA. Finally, the second grid radiates into the third grid (the upper in Fig. 13) by means of another Huygens surface. This grid is fine to accurately model the receiving antenna.

It is obvious that with the Huygens surfaces in Fig. 13, the calculation is only valid for sources in the lower volume. Concerning the approximations in the FDTD implementation, they lie in the coarse models of the antennas in the second grid. In particular, the field picked up around the receiving PIFA in that grid is only an approximation of the field which would be produced if the PIFA where modeled by the fine grid. The quality of the approximation probably depends on the distance between the antenna and the Huygens surface. The application of the method in [31] shows a very good agreement with measurements on the same model of the human body as the one used in the calculation. The method has been also applied successfully to other applications in [30, 32]. It is simpler than the HSG method, and well suited for one-way problems.

IV-4. The TF/SF method with evanescent waves

In deriving both the TF/SF connecting conditions and the equivalence theorem, the sole assumption is that the field is a solution of the Maxwell equations. From this, the TF/SF method developed for traveling waves is still valid for evanescent fields. An experiment is reported in [19] where the TF/SF method generates the well known evanescent wave that occurs behind an interface in the case of total reflection of the incident traveling wave. More recently, the TF/SF method has been used to generate evanescent plane waves in free space [33].

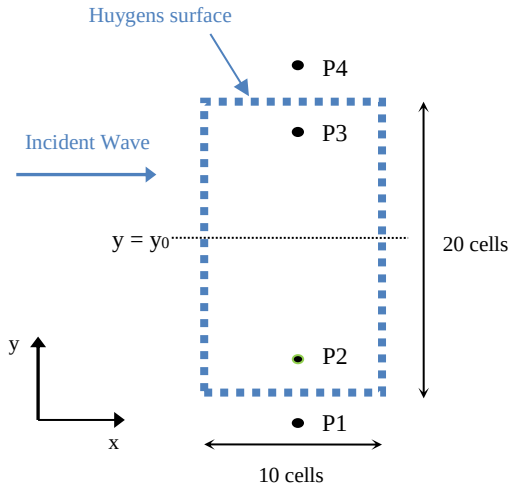

Fig. 14. FDTD computational domain for numerical experiments with evanescent waves (Δx = Δy = 5 cm, Δt = 0.1 ns). The incident wave is evanescent in *y* direction and its phase propagates in *x* direction.

Evanescent plane waves [34] are waves whose magnitude decreases exponentially in the direction perpendicular to the direction of propagation of the phase. For *x*-directed propagation and y-directed evanescence, the waveform reads

$$\psi(x,y,z) = \psi_0 \, e^{-j\frac{\omega}{c}\cosh\chi\, x} \; e^{-\frac{\omega}{c}\sinh\chi\, y} \qquad (15)$$

where ψ is any component of the field and χ is the evanescence coefficient (χ = 0 for pure traveling waves). Two modes can exist in free space, the TM mode and the TE mode [33, 34]. In both cases the electromagnetic field has a component parallel to the direction of propagation. The components of the TM mode read

$$E_{x0} = j\, Z_0 \sinh\chi \; H_0 \qquad (16a)$$

$$E_{y0} = Z_0 \cosh\chi \; H_0 \qquad (16b)$$

$$H_{z0} = H_0 \qquad (16c)$$

where Z_0 is the impedance of free space and H_0 an arbitrary constant. The wave has two components in the plane perpendicular to the propagation, E_y and H_z, and component E_x parallel to the propagation, out of phase with $\pi/2$. From (15), the magnitude of the components decrease in *y* direction, and the rate of decrease is frequency dependent.

A single frequency evanescent wave has been implemented in [33] on a Huygens surface (Fig. 14). Its magnitude H_0 is $100/Z_0$ A/m at $y = y_0$ in Fig. 14, the evanescence coefficient is $\cosh\chi$ = 1.3, and the period is 50 time steps. The implementation is the same as with a traveling wave, except that there is an additional component in the direction of propagation *x*, out of phase with $\pi/2$, and that the magnitude of the incident field decreases in *y* direction.

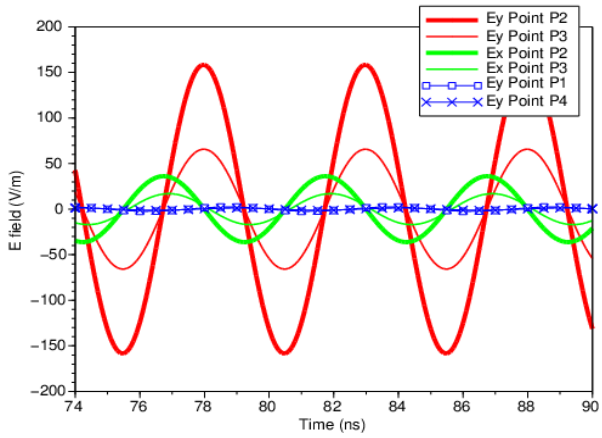

Fig. 15. Electric field inside and outside a Huygens surface generating a sinusoidal TM evanescent field.

Field components E_x and E_y at locations P1, P2, P3, P4 in Fig. 14 are plotted in Fig. 15. Field E_y at P1 and P4, out of the Huygens surface, is the leakage. It is small, although slightly larger than that of a pure traveling wave. Inside the surface, at P2 and P3, both E_x and E_y agree very well with the theoretical values from (15)-(16). The ratio of E_y at P2 and P3 is 0.415, in accordance with the theoretical ratio from (15) which is 0.4155 with $\cosh\chi$ = 1.3 and the separation between P2 and P3 (17 cells). And the E_x component is in advance with $\pi/2$ with respect to E_y, in accordance with the *j* factor in (16). This experiment demonstrates that evanescent waves can be generated by the TF/SF method, in the same way as pure traveling waves. Here the incident wave is a sinusoidal wave. Time domain evanescent pulses can be generated as well as demonstrated in [33].

V. Conclusion

The total field/scattered field method is nowadays a basic feature of FDTD simulation softwares. It is used in the numerous applications of the FDTD method where an incident field is produced by sources located outside the computational domain, and in many other applications, such as the connection of several FDTD grids.

In the first part of the paper the principle and the implementation of the method are summarized in the case of the generation of an incident traveling plane wave in a FDTD domain filled with a vacuum. In the second part the techniques developed to reduce the spurious effect of the dispersion are reviewed, mainly the AFP method [12] and the DPW method [13]. They permit extremely high dynamic range to be achieved in the computational domain. Finally, the third part is a review of the extensions and other uses of the method, introduced over the years to generate an incident wave in lossy or dispersive media, to replace a source in the FDTD domain, to connect several FDTD grids, and to generate evanescent plane waves in the FDTD domain.

REFERENCES

[1] D.E. Merewether, "Transient currents induced on a metallic body of revolution by an electromagnetic pulse", *IEEE Trans. Electrom. Compat*., vol. 13, pp. 41-44, 1971.

[2] R. Holland, "THREDE: A free-field EMP coupling and scattering code", *IEEE Trans. Nuc. Sc*., vol. 24, pp. 2416-2421, 1977.

[3] R. Holland, L. Simpson, K.S. Kuntz, "Finite-Difference Analysis of EMP Coupling to Lossy Dielectric Structures", *IEEE Trans. Electrom. Compat*., vol. 22, pp. 203-209, 1978.

[4] D.E. Merewether, R. Fisher, F.W. Smith, "On Implementing a Huygens Source Scheme in a Finite Difference Program to Illuminate Scattering Bodies", *IEEE Trans. Nucl. Sc*., vol. 27, pp. 1829-1834, 1980.

[5] K. Umashankar, A. Taflove, "A Novel Method to Analyze Electromagnetic Scattering of Complex Objects", *IEEE Trans. Electrom. Compat*., vol. 24, pp. 397-405, 1982.

[6] R. Holland, J.R. Williams "Total-field versus scattered-field finite-difference : a comparative assessment ", *IEEE Trans. Nuc. Sc.*, vol. 30, pp. 4583-4588, 1983.

[7] J.A. Kong, "Theory of Electromagnetic Waves", John Wiley & Sons, 1975.

[8] A. Taflove, "Computational Electrodynamics. The Finite-Difference Time-Domain Method", Artech House, 1995.

[9] C. Guiffaut and K. Mahdjoubi, "A perfect wideband plane wave injector for FDTD method," *Proc. IEEE APS Intl. Symp.*, Vol. 1, Salt Lake City, UT, 2000, pp. 236-239.

[10] U. Oguz and L. Gurel, "Interpolation techniques to improve the accuracy of the plane wave excitations in the finite difference time domain method," *Radio Sci.*, vol. 32, pp. 2189-2199, 1997.

[11] U. Oguz and L. Gurel, "An efficient and accurate technique for the incident-wave excitations in the FDTD method," *IEEE Trans. MTT*, vol. 46, pp. 869-882, 1998.

[12] J.B. Schneider, "Plane waves in FDTD simulations and a nearly perfect total-field/scattered-field boundary," *IEEE Trans. Ant. Propag.*, vol. 52, pp. 3280-3287, 2004.

[13] T. Tan and M. Potter, "FDTD discrete plane wave (FDTD-DPW) formulation for a perfectly matched source in TF/SF simulations," *IEEE Trans. Ant. Propag.*, vol. 58, pp. 2641-2648, 2010.

[14] A. Taflove, *Advances in FDTD Computational Electromagnetics*, Artech House: Boston, 2013.

[15] P. Wong, G. Tyler, J. Baron, E. Gurrola, and R. Simpson, "A three wave FDTD approach to surface scattering with applications to remote sensing of geophysical surfaces," *IEEE Trans. Ant. Propag.*, vol. 44, no. 4, pp. 504–14, 1996.

[16] T.-T. Hsu and L. Carin, "FDTD analysis of plane-wave diffraction from microwave devices on an infinite dielectric slab," *IEEE Microw. Guided Wave Lett.*, vol. 6, no. 1, pp. 16–18, 1996.

[17] Y. Yi, B. Chen, D.-G. Fang, and B.-H. Zhou, "A new 2-D FDTD method applied to scattering by infinite objects with oblique incidence", *IEEE Trans. Electromagn. Compat.*, vol. 47, no. 4, pp. 756–62, 2005.

[18] S. C. Winton, P. Kosmas, and C. M. Rappaport, "FDTD simulationof TE and TM plane waves at nonzero incidence in arbitrary layered media," *IEEE Trans. Ant. Propag*., vol. 53, no. 5, pp. 1721–1728, 2005.

[19] I. R. Capoglu and G. S. Smith, "A Total-Field/Scattered-Field Plane-Wave Source for the FDTD Analysis of Layered Media", *IEEE Trans. Ant. Propag*., vol. 56, no. 1, pp.158-169, 2008.

[20] Y. Fang, L. Wu, and J. Zhang, "Excitation of Plane Waves for FDTD Analysis of Anisotropic Layered Media", *IEEE Ant. Wireless Propag. Lett.*,vol. 8, 2009.

[21] B. Abdulkareem, J.-P. Bérenger, F. Costen, R. Himeno, H. Yokota, "Huygens Excitation in Debye media in the FDTD Method", *IEEE Trans. Ant.. Propag.* , 2016. DOI 10.1109/TAP. 2016. 2569198.

[22] J.-P. Bérenger, "Improved PML for the FDTD solution of wave-structure interaction problems*", IEEE Trans. Ant. Propag*., vol. 45, pp. 466-473, 1997.

[23] V. Anatha and A. Taflove, "Efficient modeling of infinite scatterers using a generalized total-field/scattered-field FDTD boundary partially embedded within PML", *IEEE Trans. Ant. Propag.*, vol. 50, no. 10, 2002.

[24] J.-P. Berenger, "FDTD computation of VLF-LF propagation in the Earth-Ionosphere waveguide", *Annals of Telecom*., vol. 57, no 11-12, pp. 1059-1090, 2002.

[25] J.-P. Bérenger, "A Huygens Subgridding for the FDTD Method", *IEEE Trans. Ant. Propag.*, vol. 54, pp. 3797-3804, 2006.

[26] J.-P. Bérenger, "Extension of the FDTD Huygens Subgridding Algorithm to two dimensions", *IEEE Trans. Ant. Propag.*, vol. 57, pp. 3860-3867, 2009. DOI 10.1109/TAP.2009.2031906.

[27] F. Costen and J.-P. Bérenger "Extension of the FDTD Huygens Subgridding to frequency dependant media" *Annals of telecom*, Oct. 2009, DOI 10.1007/s12243-009-0131-0.

[28] J.-P. Berenger, "The Huygens subgridding for the numerical solution of the Maxwell equations", *J. Comput. Phys*., vol. 230, pp. 5635-5659, 2011, DOI 10.1016/J.JCP2011.03.046.

[29] M. Abalenkov, F. Costen, J.-P. Bérenger, R. Himeno, H.Yokota, M. Fujii, "Huygens Subgridding for 3D Frequency-Dependent Finite-Dfference Time-Domain Method*", IEEE Trans. Ant. Propag*., vol. 60 , no. 9, pp. 4336-4344, 2012.

[30] R. Pascaud, R. Gillard, R. Loison, J. Wiart, and M. F. Wong, "Dual-grid finite-difference time-domain scheme for the fast simulation of surrounded antennas," *Microw. Ant. Propag.*, vol. 1, no. 3, pp. 700–706, 2007.

[31] C. Miry, Th. Alves, R. Gillard, J.-M. Laheurte, R. Loison, and B. Poussot, 'Analysis of transmission between on-body devices using the bilateral dual-grid FDTD technique", *IEEE Ant. Propag. Lett*., vol. 9, pp. 1073-1075, 2010.

[32] C. Miry, R. Loison, R. Gillard, "An efficient bilateral dual-grid-FDTD approach to on-body transmission analysis and specific absorption rate calculation", *IEEE Trans. Microw. Th. Techn*., vol. 58, no 9, pp. 2375-2382, 2010.

[33] J.-P. Bérenger, "Total-Field/Scattered-Field method for the generation of evanescent plane waves in the FDTD domain", to be submitted.

[34] G.S. Smith "An Introduction to Classical Electromagnetic Radiation", Cambridge Univ. Press, 1997.

Mike Potter received the B. Eng. in engineering physics (electrical) from the Royal Military College of Canada, Kingston, ON, Canada, in 1992, and the Ph.D. degree in electrical engineering from the University of Victoria, Victoria, BC, Canada, in 2001.

From 1992 to 1997, he served as an officer in the Canadian Navy as a Combat Systems Engineer. After completing his service and attaining the rank of Lieutenant (Navy), he completed his doctoral work in Victoria, BC, Canada. He was then a post-doctoral fellow at the University of Arizona, Tucson, AZ, USA, from 2001 to 2002. He currently holds the position of Associate Professor in the Department of Electrical and Computer Engineering at the University of Calgary, Calgary, AB, Canada. His research interests include computational electromagnetics and the FDTD method.

Dr. Potter was co-winner of the IEEE Antennas and Propagation Society 2011 Schelkunoff Prize Paper Award. He is a Senior member of the IEEE and serves as a member of the IEEE-APS Education Committee.

Jean-Pierre Bérenger received a Master in Physics from the University Joseph Fourier, Grenoble, France, in 1973, and a Master in Optical Engineering from the Institut d'Optique Graduate School, Paris, France, in 1975.

He has been with the French Ministry of Defense from 1975-2013, where he held such positions as research engineer, expert on the electromagnetic effects of nuclear bursts, and contract manager. His technical works were mainly focused on the nuclear electromagnetic pulse and on the propagation of radiowaves in nuclear environments. He performed researches on the FDTD method, the absorbing boundary conditions, and the low frequency (VLF-LF) propagation.

Jean-Pierre Bérenger is currently a consultant on the electromagnetic effects of nuclear rays and on numerical electromagnetics, and a visiting professor at the School of Electrical and Electronic Engineering, the University of Manchester, UK. He is a Fellow of the IEEE. He received the 2013 Medal of URSI-France and the 2014 John Howard Dellinger Gold Medal from URSI.